SAND2025-12376J

npj | advanced manufacturing

Article

https://doi.org/10.1038/s44334-025-00032-1

# Real-time process monitoring and automated control for direct ink write 3D printing of frontally polymerizing thermosets



Edgar B. Mejia[1,2], Luke McDougall[1], Nicolas Gonsalves[3], Daniel R. Darby[1], Andrew J. Greenlee[1], Alex Commisso[1], Jeremiah A. Johnson[4], Nancy Sottos[2], Leah N. Appelhans[1], Adam W. Cook[1], Samuel C. Leguizamon[1] & Devin J. Roach[1,3] ✉

Additive manufacturing (AM) enables the fabrication of complex geometries, yet its application to thermosets remains limited by post-processing requirements. Frontal ring-opening metathesis polymerization (FROMP) offers a promising alternative, enabling energy-efficient, in situ curing of freestanding thermoset structures. This study presents a real-time process monitoring and automated control system for direct ink writing (DIW) of FROMP thermosets. By integrating thermochromic leuco dyes and computer vision, we enable real-time polymerization front tracking, allowing autonomous printing parameter adjustments for consistent geometries across resin formulations. The system's accuracy was validated against manual tracking, demonstrating precise front velocity detection. Its adaptability was confirmed by printing freestanding mechanical springs with different resins, achieving consistent geometries and mechanical properties despite front velocity variations. These findings highlight the potential of automated DIW control for scalable, repeatable, and material-agnostic 3D printing of thermosets.

Additive manufacturing (AM) has transformed the field of manufacturing by providing unprecedented design flexibility, accelerating design cycles, and enabling the creation of intricate 3D geometries. The most commonly used AM materials are thermoplastics, which are simple to process but often suffer from poor mechanical properties, especially in variable thermal environments, rendering them unsuitable for high-performance applications such as automotive or aerospace[1]. In contrast, thermoset polymers offer reliable thermomechanical properties, chemical stability, and straightforward polymerization strategies[2–4]. Recent advances in thermoset compositions and polymerization techniques have enabled AM of thermosets with nearly unlimited access to an array of mechanical[5], thermal[6,7], and dielectric properties[8,9]. Among the various AM methods for fabricating thermoset polymers, direct ink writing (DIW) 3D printing—an extrusion-based technique—has emerged as the most material agnostic[10]. DIW stands out due to its ability to fabricate intricate structures from a wide range of materials while maintaining low material consumption and cost. Researchers have employed DIW to fabricate intricate thermoset structures, including lattice metamaterials[9], core-shell structures[11,12], self-supporting architectures[13–15], and shape-morphing objects[16–18]. Despite the advantages of DIW, post-curing with ovens or high-intensity UV lights is often required, limiting its feasibility for on-demand, in situ fabrication.

Frontal polymerization is a promising approach for the rapid manufacturing of thermosets, utilizing the exothermic enthalpy of polymerization to provide the energy to propagate the polymerization, eliminating the need for an external energy source[19]. One type of frontal polymerization, called frontal ring-opening metathesis polymerization (FROMP), was introduced in 2001 to polymerize polydicyclopentadiene (pDCPD) to prepare high-performance thermosets using commercially available reagents[20]. In 2018, Robertson et al. demonstrated the potential of frontal polymerization as a more energy-efficient and faster alternative to traditional curing methods for high-performance thermoset polymers and composites[21]. Using this approach, Sottos and colleagues demonstrated that frontal polymerization could be used for DIW 3D printing of self-curing thermoset polymers[22]. By carefully tuning the nozzle velocity to match the polymerization front

[1]Advanced Materials Laboratory, Sandia National Laboratories, Albuquerque, NM, USA. [2]Materials Science & Engineering, University of Illinois at Urbana-Champaign, Champaign, IL, USA. [3]Mechanical, Industrial, & Manufacturing Engineering, Oregon State University, Corvallis, OR, USA. [4]Chemistry, Massachusetts Institute of Technology, Cambridge, MA, USA. ✉e-mail: devin.roach@oregonstate.edu

velocity (referred to as the front velocity), they demonstrated the printing and in situ curing of freestanding thermoset architectures, capable of spanning gaps up to 100 mm to create architectures previously unattainable with other thermoset DIW methods. This technique has since been expanded to produce a range of new components, including carbon fiber-reinforced composites[23], tailorable stretchable thermosets[24], and shape memory structures[13]. Nevertheless, limited regulation of frontal polymerization during printing has been demonstrated through a complex thermal environment with a cooled syringe and heated print bed, introducing additional power requirements and the need for specialized tooling. Automated control of printing parameters, such as extrusion rate and nozzle velocity during DIW, could address this issue, but it remains a significant challenge.

The most promising approach to automated control of DIW involves using cameras to capture real-time information about the printing process, which can then be used to inform process optimization steps[25,26]. This approach is called computer vision and, when combined with big data, can enable real-time control strategies to adjust printing parameters dynamically[27,28]. Nonetheless, measuring frontal polymerization for thermosets during the DIW process has not been demonstrated apart from in-line IR sensors[29]. Therefore, a straightforward method for measuring thermoset cure kinetics is critical for real-time adjustment of DIW 3D printing parameters.

In this work, a computer vision-based approach was developed for the automated measurement of frontal polymerization in thermosets, enabling real-time control of DIW 3D printing parameters to produce high-quality components for a variety of printed materials. High-resolution cameras operating at 200 Hz captured real-time images of the frontal polymerization process, with image analysis performed using Python-based computer vision toolboxes to filter the data and accurately track the polymerization front. The incorporation of thermochromic leuco dyes, which change color as a result of temperature change, significantly improved the detection of the polymerization front without affecting the front velocity or the mechanical properties of the printed materials. The front velocity was easily determined by tracking the front's movement over time. This method was applied across various resin systems with distinct front velocities, allowing real-time printing process optimization to match the front velocity with the nozzle velocity. Lastly, we demonstrate the effectiveness of this approach through the DIW printing of freestanding spring architectures using two different resins. Despite differences in resin properties, the automated front detection and process optimization ensured consistent geometry and force-displacement behavior across both prints. This auto-regulated approach for extrusion 3D printing of frontal polymerized gels offers a promising solution for repeatable, scalable, and sustainable fabrication of complex 3D thermoset structures with high precision and resolution, regardless of the material formulation.

## Results

### Thermochromic dye incorporation in FROMP

The study initially explored the effect of a thermochromic dye on a well-characterized resin used in FROMP[21]. The FROMP formulation comprised three key components: (1) a ring-strained monomer, dicyclopentadiene (DCPD), which undergoes frontal polymerization; (2) a catalyst, such as the second-generation Grubbs catalyst (GC2), responsible for initiating the polymerization; and (3) an inhibitor, like tributyl phosphite (TBP), used to control the reaction rate by regulating the catalyst's activity (Fig. 1a). The thermochromic leuco dye was introduced into the resin to visualize the polymerization front, changing color from black below 35 °C to vibrant pink above 35 °C (Fig. 1b). DIW of these inks was performed using a custom-built printer and a real-time control environment previously described in related studies demonstrating DIW of unique thermoset polymer resins[28,30,31]. Figure 1c schematically illustrates printing of frontally polymerized p(DCPD). Notably, the addition of up to 2 wt% dye did not affect the thermomechanical properties, such as storage modulus and glass transition temperature, as confirmed by dynamic mechanical analysis (DMA) (Fig. 1d). A detailed discussion of the dye's impact on detection accuracy is provided in the following sections.

### Adaptive process control for DIW 3D printing

A high-resolution camera, mounted parallel to the extrusion nozzle, was integrated into the printer setup to determine the front velocity (Fig. SI1). In this study, front velocity refers to the propagation speed of the exothermic

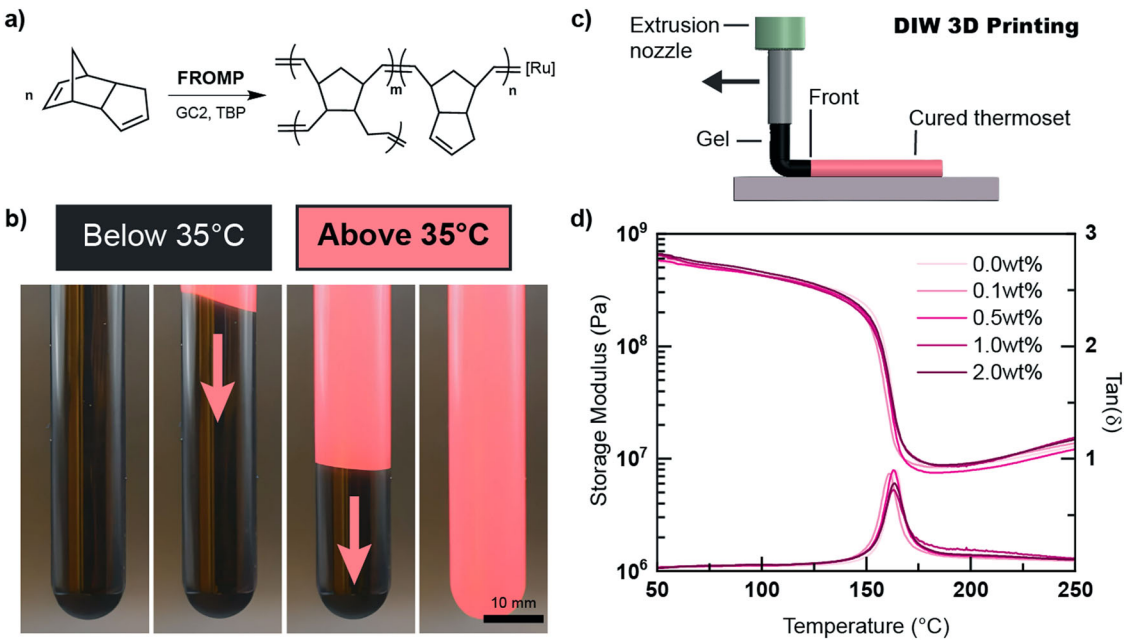


**Fig. 1 | Addition of thermochromic dye to thermosetting polymer resin for simple polymer front detection during DIW 3D printing. a** Frontal ring-opening metathesis polymerization (FROMP) of DCPD [monomer], GC2 [catalyst], TBP [inhibitor]. **b** Front propagation in a thermochromic dye-loaded resin, showing a color change from black to pink. **c** Schematic of the DIW 3D printing system showing FROMP curing following the printing path. **d** Thermomechanical properties of pDCPD with varying thermochromic dye loadings characterized by DMA.

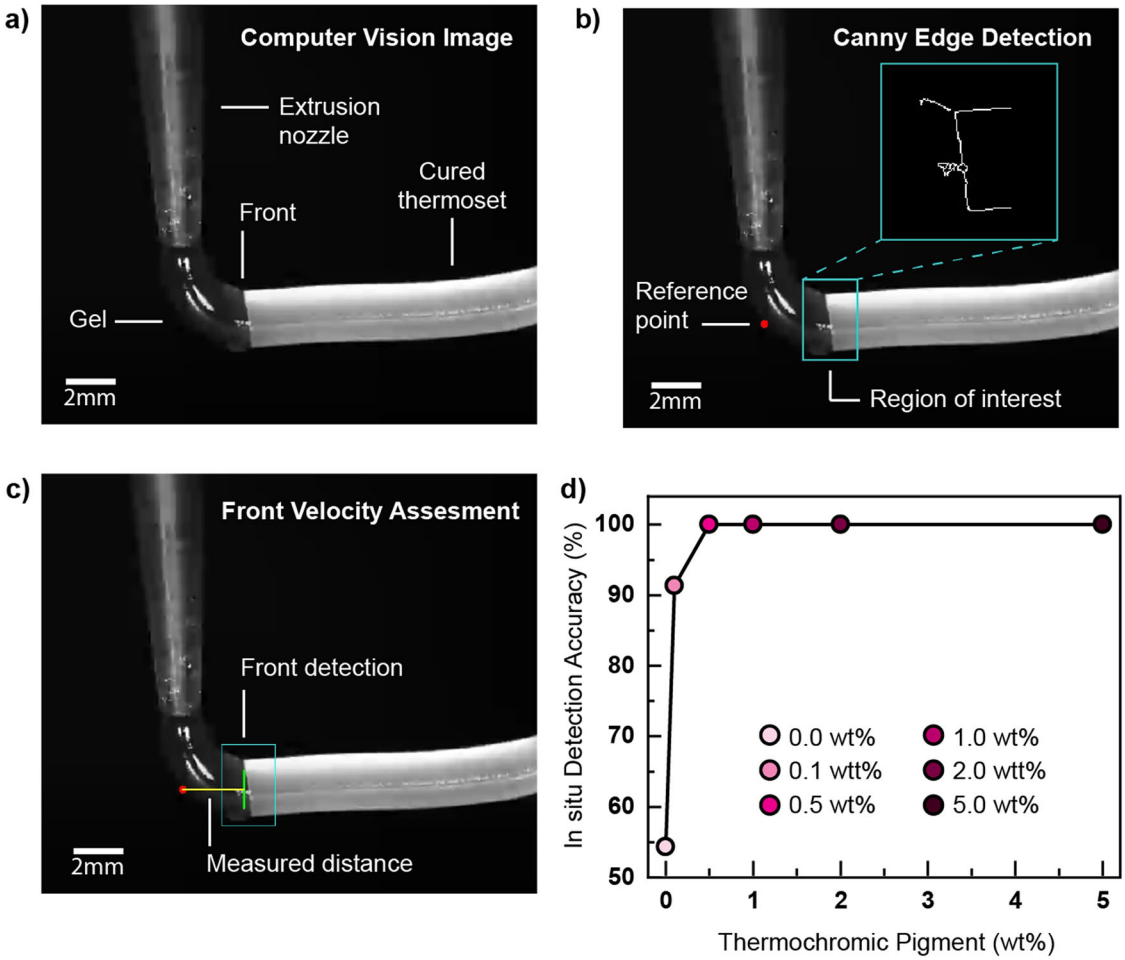


**Fig. 2 | Computer vision approach for automated polymerization front detection. a** Black and white still image of DIW 3D printing of p(DCPD) with thermochromic dye during curing. **b** Edge detection processing on the region of interest and reference point. **c** Automatized front detection and distance determination for front velocity calculation. **d** In situ detection accuracy for different thermochromic loading.

polymerization reaction zone, which separates the fully cured thermoset from the monomer ink. Red lights were focused on the DIW print head to maintain constant illumination, reduce undesired reflections, and increase contrast. This setup allowed the camera and lights to move in tandem with the printing nozzle. Before printing, a pixel-to-mm calibration was performed to ensure accurate measurement of the frontal polymerization and printing rates. Videos were captured at a rate of 200 frames per second, enabling precise tracking of the propagating front. An image acquired by the computer vision cameras during FROMP with thermochromic dye distinctly shows the difference between the extruded gel and the cured polymer (Fig. 2a).

A Python script was used to filter the real-time images, determine the velocity of the front, and automatically update the 3D printing parameters during the printing process. A detailed workflow of the Python script can be seen in Fig. SI2. The first step was that each frame underwent edge detection, which transforms an image into a binary representation, emphasizing the boundaries of objects with contrasting black and white colors. Additionally, black-and-white thresholds for this specific system were optimized for contrast and noise reduction. A reference point was placed underneath the extrusion nozzle in each frame, and a region of interest (ROI) encompassing a rectangular area of 60 × 80 pixels was set 30 pixels away from the reference point (Fig. 2b). An algorithm then analyzed the ROI to detect a linear front based on specific criteria, including a minimum line length (30 pixels), a maximum edge slope (15 degrees from vertical), and a maximum gap between edges (7 pixels) to account for unwanted reflections (Fig. SI3).

Once a linear front was detected within the ROI, the system measured the distance between the detected front and the reference point at a rate of 100 Hz (Fig. 2c). Each distance measurement was recorded, and the system then calculated the difference between the first and last value measured over half second intervals to determine the front velocity. The nozzle velocity was then automatically adjusted to match the measured front velocity, ensuring the front remained at a consistent distance from the reference point. Because nozzle velocity alone does not dictate material output, we employ a coupled control scheme that synchronizes changes in nozzle velocity with proportional adjustments to the extrusion rate, providing a consistent volumetric flow. This approach mitigates the risk of under- or over-extrusion when responding to fluctuations in the polymerization front velocity. This process operated continuously, capturing new frames, performing edge detection and front detection within the ROI, measuring the distance between the front and the reference point, calculating the front velocity, and updating the nozzle velocity. A video of the system performing real-time auto-regulative printing using this approach can be seen in SI Video 1. The system started with a nozzle velocity of 1 mm $s^{-1}$; if no front was detected within a second, the system reduced the printing velocity by 25%, allowing the lagging front to catch up to the nozzle. This framework is crucial for automatically printing various formulations without requiring prior knowledge of the front velocity.

### Optimizing dye loading for accurate front detection

After refining the system workflow, we evaluated the effect of thermochromic dye concentration on detection accuracy. Accurate detection of

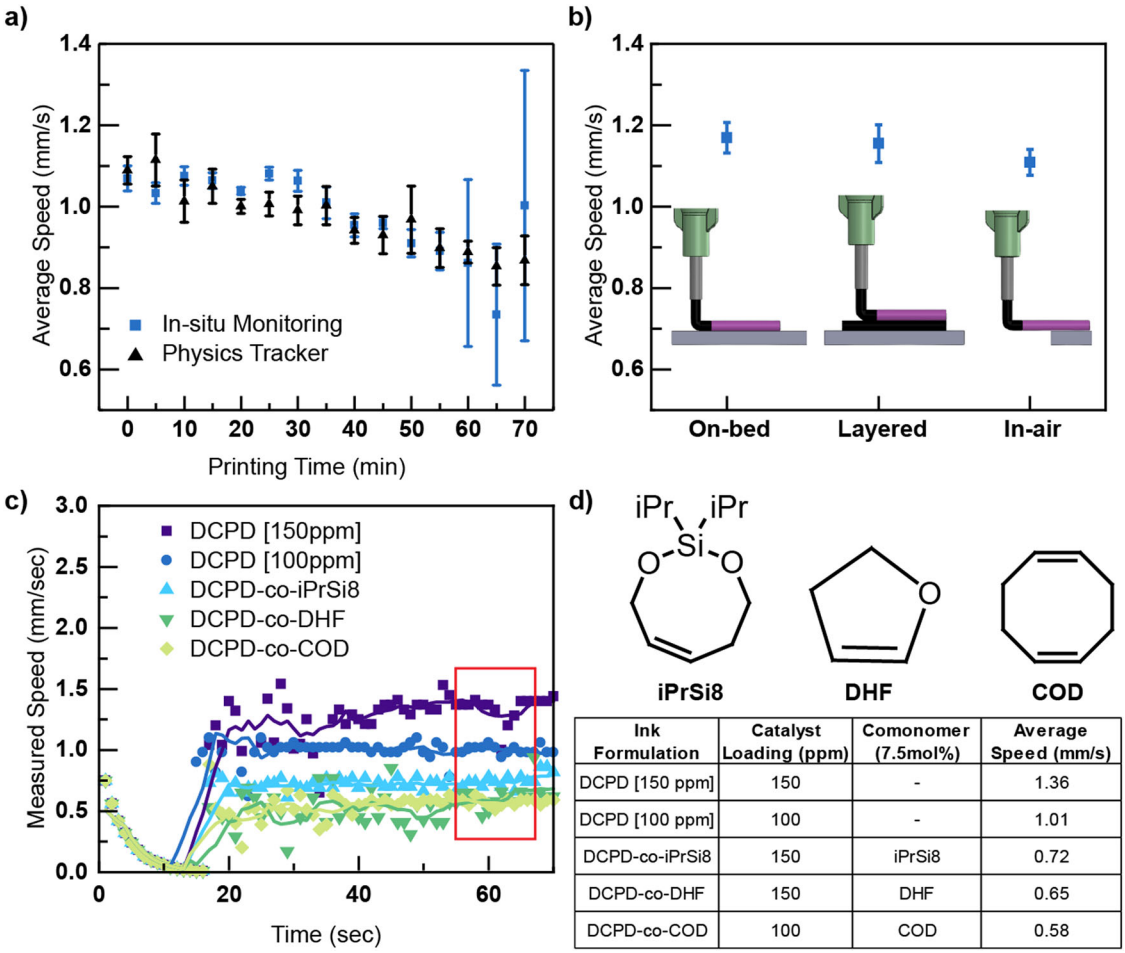


| Ink Formulation | Catalyst Loading (ppm) | Comonomer (7.5mol%) | Average Speed (mm/s) |
|---|---|---|---|
| DCPD [150 ppm] | 150 | - | 1.36 |
| DCPD [100 ppm] | 100 | - | 1.01 |
| DCPD-co-iPrSi8 | 150 | iPrSi8 | 0.72 |
| DCPD-co-DHF | 150 | DHF | 0.65 |
| DCPD-co-COD | 100 | COD | 0.58 |

**Fig. 3 | Automated polymerization front velocity detection and characterization for varying print scenarios and resin formulations. a** Comparison of average velocities between the in situ monitoring system and a physics tracker. **b** Average front velocities under different printing conditions. **c** Front velocity measurements for various resin formulations. **d** Velocity comparisons across different catalyst loadings and comonomer formulations ($n = 3$).

the propagating polymerization front is crucial for precise control over the 3D printing process. Different inks were prepared with varying amounts of thermochromic dye, and front detection accuracy during 5 s (50 frames) of recording was manually verified. Positive front detections were counted over that period, false positive readings were removed, and the number of accurate front detections was divided by the total number of frames to obtain an accuracy percentage. This approach exhibited a 54% accuracy for pure pDCPD thermosets as slight color changes occur during polymerization of pure pDCPD thermosets (Fig. 2d). However, with a small addition of thermochromic dye (0.1 wt%), the accuracy increased dramatically to 91.33%. The accuracy reached 100% by adding 0.5 wt% thermochromic dye loading and reaching a plateau at higher loadings. Therefore, the addition of thermochromic dye provides a clear distinction between the extruded gel ink and the polymerized thermoset, allowing for facile detection of the self-propagating polymerization front during DIW 3D printing. Based on these results and the thermo-mechanical characterization previously discussed, 0.5 wt% was determined to be the optimal thermochromic dye loading.

### Influence of resin aging on front velocity and detection accuracy

Background polymerization enables the ink to reach a viscosity suitable for DIW 3D printing. However, as the ink continues to polymerize, it undergoes rheological changes that can potentially affect front velocity. To understand the influence of the evolving gel state on the accuracy of the in situ monitoring system, a line was extruded every 5 min from a single batch of resin over a span of 70 min (Fig. 3a). The front velocity measured by the system was then compared to that obtained using open-source physics tracking software. As anticipated, the results showed a decrease in front velocity over time, attributed to monomer consumption, which reduces the residual heat of polymerization in FROMP[21]. The in situ monitoring system accurately measured front velocity during the first 55 min of printing. However, after 60 min, a significant increase in measurement variability was observed. We propose that this variability is due to a phenomenon known as "sharkskin" in the 3D-printed specimens, characterized by periodic surface irregularities. Although widely studied, the exact cause of this instability remains under debate, with a prevalent theory suggesting localized stress-induced polymer fracture at the die exit as the ink shears against the nozzle wall during extrusion[32,33]. These ridge-like irregularities cause undesired reflections, which the in situ monitoring system incorrectly identifies as front locations (Fig. SI4). As a result, the standard deviation of front velocity measurements increases significantly, leading to a decrease in detection accuracy above 55 min.

To further explore the versatility of the in situ monitoring system, linear prints were performed under three different conditions: directly on a build platform ("on-bed"), on a previously printed layer ("layered"), and in free space without a supporting structure ("in-air"). The front velocity did not differ significantly across these conditions (Fig. 3b). This finding is crucial, as it demonstrates the system's ability to accurately determine front velocity under various conditions and maintain matching print speed during printing of complex geometries, including in-air printing. This capability is particularly valuable when support structures are impractical or undesirable.

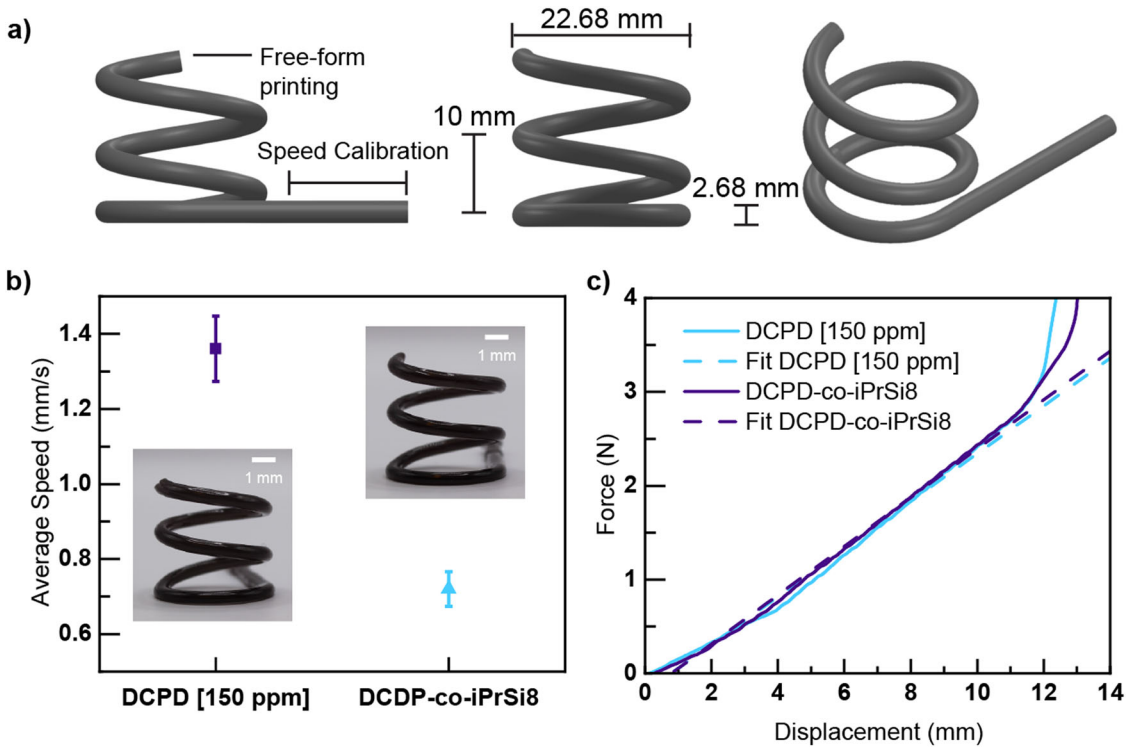


**Fig. 4 | Automated free-form 3D printing of springs using distinct FP inks which achieve identical geometry and spring constants despite different frontal polymerization rates. a** Schematic of 3D-printed spring, highlighting the linear section and the freeform unsupported section. **b** Average front velocities and corresponding images of 3D-printed spirals using DCPD [150 ppm] and DCPD-co-iPrSi8 inks. **c** Compression testing results, showing that both printed spirals achieve the same spring constant despite differences in material composition.

### Dynamic adjustment of printing parameters for different resin systems

To evaluate the adaptability of the in situ process control system across various resin formulations, catalyst loading was varied, and three comonomers were introduced, which were expected to alter the front velocity of FROMP (Table SI5). A moving average was used to display the system's automatic front velocity tracking and the corresponding adjustments to the printing nozzle velocity (Fig. 3c). As detailed in Adaptive Process Control for DIW 3D Printing, the process begins with the nozzle moving at 1 mm $s^{-1}$, while a soldering iron is used to initiate front propagation. Initially, a brief decrease in nozzle velocity was observed due to the absence of a detectable front in the ROI. The system then rapidly increased the nozzle velocity to match the polymerization front velocity. While the extrusion rate is coupled to the nozzle velocity, the lack of a retraction feature allows die swell effects to form a non-uniform material reservoir. This initially leads to fluctuations in the printing velocity (Fig. SI6). However, the system self-corrected, eventually reaching a stable state. Maintaining an appropriate extrusion rate is critical for ensuring a stable polymerization front. Under-extrusion reduces the volume-to-surface area ratio of the cured thermoset, increasing heat dissipation and raising the risk of front quenching. Conversely, over-extrusion can introduce inconsistencies in material deposition, potentially destabilizing the polymerization front. The average front velocity and corresponding printing speeds of the different inks were measured over 10 s of unsupported printing, with three replicates performed for each formulation.

First, formulations with catalyst loadings of 100 ppm and 150 ppm of DCPD were tested. The system automatically adjusted the nozzle velocity to match the front velocity, irrespective of catalyst concentration. Videos of the front identification and self-adaptive printing approach for 150 ppm and 100 ppm inks can be seen in SI Videos 1 and 2, respectively. The front velocity increased from 1.01 mm $s^{-1}$ for the 100 ppm formulation to 1.36 mm $s^{-1}$ for the 150 ppm formulation. The observed phenomenon of front velocity increase with higher catalyst loading aligns with previously published data[34]. Inks incorporating comonomers were printed to further demonstrate our in situ monitoring system's versatility. One such resin, containing 7.5 mol% of 2,3-dihydrofuran (DHF), had been reported to exhibit a slower front velocity[35]. Our system measured an average front velocity of 0.65 mm $s^{-1}$, closely matching the previously reported value of 0.54 mm $s^{-1}$.

A formulation incorporating 1,5-cyclooctadiene (COD) as a comonomer with DCPD was evaluated to demonstrate the system's capability with novel resin compositions. To our knowledge, COD has never been used in a DIW process, despite its established role in modifying polymer properties when combined with DCPD[6]. The ratio of COD to DCPD significantly influences both the thermomechanical properties of the polymer and the front velocity of FROMP. Incorporating 7.5 mol% COD into the DCPD formulation reduced the front velocity to an average of 0.58 mm $s^{-1}$, compared to the control DCPD formulation at the same catalyst loading.

Finally, we tested a formulation incorporating an eight-membered cyclic silyl ether comonomer (iPrSi8), previously used as a cleavable comonomer in p(DCPD) formulations[36,37]. iPrSi8 integrates into the polymer network backbone, enabling efficient deconstruction at low comonomer loadings for future upcycling[38]. However, to our knowledge, iPrSi8 has never been used in a 3D printing process. The in situ monitoring system demonstrated effective adaptability across various resin formulations, accurately tracking the front velocity and adjusting the printing nozzle velocity in real-time. This capability was consistent across different catalyst loadings and comonomers, including novel formulations, highlighting the system's versatility for 3D printing complex and high-performance thermosets. These results emphasize the potential of this approach for future advancements in AM and upcycling of thermosets.

### Enabling complex, high-precision structures through automated control

Finally, we evaluated the in situ monitoring system's ability to produce reproducible geometries across different resin systems by printing

freestanding mechanical springs. A schematic of an unsupported 3D-printed spiral with two distinct sections is shown below in Fig. 4a. Here, the first section consists of a 17 mm linear path that allows the in situ monitoring system to measure the front velocity of the ink and adjust the printing parameters before printing the second, freestanding spring section. Importantly, to maintain high dimensional accuracy throughout the printing process, the printing nozzle velocity must match the front propagation speed during FROMP, as shown in Fig. SI7 and SI Video 3.

Two different formulations with the same catalyst loading were selected for this demonstration. Although DCPD [150 ppm] exhibited the fastest velocity among all the tested inks (1.36 mm $s^{-1}$), an almost identical geometry was achieved using a much slower ink, DCPD-co-iPrSi8, which moved at half the velocity (Fig. 4b). Compression testing was conducted to demonstrate the impressive geometric similarity between the two printed springs. The spring constant can be calculated by fitting the slope of the linear region of the force vs. displacement curve (Fig. 4c). Both springs presented similar values, 254.4 $Nm^{-1}$ for DCPD [150 ppm] and 260.1 $Nm^{-1}$ for DCPD-co-iPrSi8. The predicted spring constant based on geometry could also be calculated using principles of spring design[39], as shown in the equation below:

$$k = \frac{Gd^4}{8D^3 n_a}$$

where $G$ represents the shear modulus of the material, $d$ is the spring wire diameter, $D$ is the mean diameter of the spring, and $n_a$ is the number of active coils. The calculated values were consistent with the experimental results, yielding a predicted value of 241.8 $Nm^{-1}$ for DCPD [150 ppm] and 245.9 $Nm^{-1}$ for DCPD-co-iPrSi8. These findings emphasize that the consistency of the spring constants, regardless of the ink's front velocity, reflects the system's ability to print highly reproducible geometries from different resins. The developed in situ monitoring system successfully adjusts printing parameters based on the ink's front velocity, enabling the precise fabrication of complex 3D-printed parts with varying resin formulations. This capability demonstrates its broad applicability for any thermoset resin system requiring adaptable front-velocity control.

## Discussion

This study demonstrates the development of an in situ, computer vision-based monitoring and control system capable of autonomously adjusting printing parameters for DIW of thermosets undergoing FROMP. By integrating thermochromic leuco dyes into the resin formulations, the system achieves reliable real-time tracking of the polymerization front, allowing the printer to respond dynamically to variations in front velocity. Importantly, the inclusion of the dye was shown to have no measurable effect on the thermomechanical properties of the final cured material yet significantly enhanced the detection accuracy of the front.

The system's performance was benchmarked against manual tracking using a commercial physics tracker, confirming its high accuracy in front velocity measurement. Unlike conventional FROMP-DIW approaches that require manual tuning of printing parameters for each resin formulation, this automated platform seamlessly adapted to a range of formulations with varying front velocities. The utility of this approach was further validated by printing freestanding mechanical springs from distinct resin systems. Despite differences in material composition and reaction kinetics, the resulting structures exhibited nearly identical geometries and mechanical performance, demonstrating the robustness of the monitoring and control system. These results suggest a high degree of process repeatability, a critical factor for translating DIW-FROMP technologies into scalable manufacturing applications.

Compared to existing frontal printing methods, the proposed strategy offers several key advantages. The closed-loop nature of the system enables continuous, real-time adjustment of printing speed and conditions in response to environmental or formulation-based changes. The use of thermochromic dyes provides a simple yet effective non-invasive solution for front tracking, eliminating the need for embedded sensors or complex instrumentation. Finally, the auto-regulative approach allows for precise printing of intricate and complex structures from diverse resin formulations. By integrating adaptive automation and removing the dependence on formulation-specific calibration, this system represents a major step forward in the control and scalability of frontal polymerization-based DIW. The demonstrated framework opens pathways toward energy-efficient, on-demand fabrication of high-performance thermosets, with potential applications spanning aerospace, printed electronics, and robotics. Future work may extend this platform through multi-angle imaging and more advanced nozzle architectures, further enhancing its responsiveness and expanding its applicability.

### Materials

All reagents were obtained from commercial sources and used as received without additional purification, unless otherwise specified. The materials used in this study include dicyclopentadiene (DCPD, Sigma-Aldrich) as the primary monomer in all resin formulations, mixed with ethylidene norbornene (ENB, TCI America) to lower its freezing point. Grubbs' second-generation catalyst (GC2, Sigma-Aldrich) was used to initiate FROMP. Tributyl phosphite (TBP, TCI America) served as an inhibitor to regulate the catalyst activity and control the reaction rate. Thermochromic leuco dye (Atlanta Chemical Engineering) was added to the resin to enable real-time visualization of the polymerization front during DIW. Additionally, several comonomers were incorporated to adjust the front velocity and properties of the resulting polymers, including 2,3-dihydrofuran (DHF, Oakwood Chemical), 1,5-cyclooctadiene (COD, Sigma-Aldrich), and an eight-membered cyclic silyl ether (iPrSi8, synthesized as described previously[40,41]) to create cleavable and deconstructable thermosets. All mentions of DCPD in this manuscript refer to a 95:5 weight ratio mixture of DCPD and ENB.

## Methods

### Ink preparation

GC2 (1 equivalent) was carefully weighed into a scintillation vial and TBP (1 equivalent) was then added. Separately, DCPD, ($6.67 \times 10^3$ or $10.00 \times 10^3$ equivalents) was measured and transferred into the vial containing the GC2 and TBP mixture. The resulting mixture was sonicated for 5 min to ensure complete dissolution of the catalyst. Comonomer resins were prepared in a similar manner, with the total monomer concentration maintained at $6.67 \times 10^3$ (150 ppm) or $10.00 \times 10^3$ (100 ppm) molar equivalents, relative to GC2. Following preparation, the inks were incubated at 25 °C in an environmental chamber to increase viscosity and ensure stable extrusion during DIW printing, following procedures established in prior work[21,22,34,35]. The iPrSi8-containing formulation followed the same incubation process. In contrast, COD-containing inks were first conditioned at 5 °C for 3 h to increase viscosity and minimize the risk of spontaneous polymerization, then transferred to a 25 °C oven for final conditioning prior to printing. Rheological properties were qualitatively assessed via vial-tip tests[42,43] and monitored periodically to ensure consistent printability across batches.

### 3D printing platform

A custom-designed DIW system equipped with a real-time control environment (Aerotech A3200) was employed to position the printing nozzle in the X-Y-Z space. A volumetric syringe pump, mounted on the Z-axis motion stage, extruded the inks during the printing process. Printing was carried out at room temperature onto an aluminum platform, coated with PTFE to prevent adhesion with the resin. A nozzle with an inner diameter of 1.55 mm was used for extrusion. The initiation of FROMP was achieved using a soldering iron set to 400 °C to provide controlled heating and induce polymerization of the DCPD.

### Computer vision system

The computer vision system comprised a Basler Ace2 (Basler AG, Ahrensburg, Germany) camera positioned at a 45-degree angle relative to

the extrusion nozzle for optimal visualization of the polymerization front. Images were captured via a CameraLink cable connected to an NI PXIe-1088 chassis, using a PXIe-1435 Frame Grabber Module (National Instruments, Austin, TX, USA). Two red lights (~650 nm) were mounted alongside the camera to move in tandem with the printing nozzle, providing consistent illumination. After image acquisition, custom computer vision algorithms developed using open-source Python libraries were applied to detect and measure the polymerization front, allowing for real-time adjustments to the printing parameters.

### Python-based computer vision

The front speed during the 3D printing process was calculated using a computer vision approach developed in Python. A pixel-to-millimeter calibration was performed using a ruler prior to testing to ensure accurate spatial measurements. Real-time monitoring of the nozzle position was achieved by selecting a ROI around the nozzle. Canny edge detection was used to identify the most notable vertical line within the ROI, representing the FROMP movement. The parameters for Canny detection, $T_{lower}$ and $T_{upper}$, were adjusted based on daily lighting variations, improving detection while minimizing false reflections. Additionally, the Hough line transformation's 'line gap' parameter was optimized to enhance line detection precision. Speed and distance data were continuously logged for analysis and real-time process optimization. The comprehensive source code employed in this research is shown in Fig. SI8.

### Accuracy detection calculation

The accuracy of FROMP line detection during the printing process was evaluated using a multi-step procedure. Initially, the true position of the polymerization front was manually analyzed on specific frames from each video recording, providing a reference for comparison. The computer vision system then automatically detected the polymerization front in the same videos. Detection accuracy was determined by comparing the system's results to the manually marked reference, measuring the difference between the two. This process was repeated across various dye concentrations (0%, 0.1%, 0.5%, 1%, and 2% by weight), with three video recordings analyzed for each concentration to ensure a comprehensive evaluation of the detection system.

### Pot life study

In the pot life study, we aimed to determine the duration over which the DCPD-based ink remained viable for DIW 3D printing and to assess the system's ongoing ability to detect the polymerization front. To do this, we printed a single line of pDCPD every 10 min, continuing until the ink exhibited noticeable degradation, including higher viscosity, reduced bed adhesion, and sharkskin defects (SI4). We ended the experiment once the in situ monitoring system could no longer reliably locate the polymerization front. By monitoring ink consistency, printability, and detection accuracy over time, this approach offered a comprehensive view of the DCPD ink's pot life and the robustness of our printing setup.

### Physics tracker

To evaluate the accuracy of the real-time front velocity tracking software developed in this study, we utilized Tracker (https://physlets.org/tracker/), an open-source video analysis and modeling tool for manual tracking of the polymerization front. Videos of the printing process were recorded, and a 10-s segment from each printed line in the pot life study was analyzed frame by frame to determine the front velocity profiles, providing a benchmark for comparison with the in situ monitoring system.

### Effect of printing conditions

We assessed the impact of different printing conditions by testing three distinct scenarios: direct printing on the print bed, printing atop a previously printed DCPD layer, and an air-printing setup. For each condition, three lines of DCPD were printed, allowing the polymerization front to reach a steady state, ensuring consistency across all tests. This standardized approach enabled accurate comparisons of performance across the varied conditions, with a focus on speed stabilization and material-substrate interaction. The data gathered from these tests provided valuable insights into how different substrates affect the printing process, particularly in relation to front propagation and the overall stability of the material during DIW 3D printing.

### Dynamic mechanical analysis (DMA)

The thermomechanical properties of pDCPD samples were evaluated using DMA on a TA Instruments RSA G2 equipped with torsion grips in ambient conditions. Standard TypeV dogbone samples with a gauge length of 7.62 mm, a width of 3.18 mm, and a thickness of 4 mm were subjected to dynamic loading at a frequency of 1 Hz. The strain amplitude was set at 0.5%. The temperature was increased linearly at a rate of 3 °C $min^{-1}$, starting from 50 °C up to 250 °C. Data were analyzed and exported using TA Instruments Trios v5 software.

### Compression testing

Compression testing of the 3D-printed springs was performed on an Instron (Norwood, MA, USA) 5564 Universal Testing Machine. Each spring was carefully aligned between the compression plates to prevent off-axis loading, and testing took place at room temperature under displacement control, with the crosshead moving at 1 mm $min^{-1}$. Force and displacement data were continuously recorded throughout the test, allowing accurate analysis of the mechanical response.

## Data availability

All data supporting the findings of this study are available within the manuscript and its Supplementary Information. The datasets generated and analyzed during this study are available from the corresponding author upon reasonable request.

## Code availability

The code used in this study is shown in Fig. SI8. A copy is also available from the corresponding author upon reasonable request.

Received: 16 December 2024; Accepted: 16 April 2025;
Published online: 12 May 2025

## References

1. Bakır, A. A., Atik, R. & Özerinç, S. Mechanical properties of thermoplastic parts produced by fused deposition modeling: a review. *Rapid Prototyp. J.* **27**, 537–561 (2021).
2. Greenlee, A. J., Weitekamp, R. A., Foster, J. C. & Leguizamon, S. C. PhotoROMP: the future is bright. *ACS Catal.* **14**, 6217–6227 (2024).
3. Gao, C., Qiu, J. & Wang, S. In-situ curing of 3D printed freestanding thermosets. *J. Adv. Manuf. Process* **4**, 462–472 (2022).
4. Wang, B., Zhang, Z., Pei, Z., Qiu, J. & Wang, S. Current progress on the 3D printing of thermosets. *Adv. Compos. Hybrid. Mater.* **3**, 462–472 (2020).
5. Kuang, X. et al. Grayscale digital light processing 3D printing for highly functionally graded materials. *Sci. Adv.* **5**, 1–9 (2019).
6. Dean, L. M., Wu, Q., Alshangiti, O., Moore, J. S. & Sottos, N. R. Rapid synthesis of elastomers and thermosets with tunable thermomechanical properties. *ACS Macro Lett.* **9**, 819–824 (2020).
7. Hartquist, C. M. et al. Reversible two-way tuning of thermal conductivity in an end-linked star-shaped thermoset. *Nat. Commun.* **15**, 5590 (2024).
8. Arrington, C. B. et al. 3D Printing carbonaceous objects from polyimide pyrolysis. *ACS Macro Lett.* **10**, 412–418 (2021).
9. Kuang, X. et al. High-speed 3D printing of high-performance thermosetting polymers via two-stage curing. *Macromol. Rapid Commun.* **39**, 1–8 (2018).
10. Elahee, G. M. F. et al. Acrylic sealants as practicable direct ink writing (DIW) 3D-printable materials. *MRS Commun.* **13**, 299–305 (2023).

11. Pack, R. C. et al. Carbon fiber and syntactic foam hybrid materials via core–shell material extrusion additive manufacturing. *Adv. Mater. Technol.* **5**, 12 (2020).
12. Mueller, J., Raney, J. R., Shea, K. & Lewis, J. A. Architected lattices with high stiffness and toughness via multicore–shell 3D printing. *Adv. Mater.* **30**, 12 (2018).
13. An, Y., Jang, J. H., Youk, J. H. & Yu, W.-R. Frontally polymerizable shape memory polymer for 3D printing of free-standing structures. *Smart Mater. Struct.* **31**, 025013 (2022).
14. Armstrong, C. D., Yue, L., Demoly, F., Zhou, K. & Qi, H. J. Unstructured direct ink write 3D printing of functional structures with ambient temperature curing dual-network thermoset ink. *Adv. Intell. Syst.* **5**, 1 (2023).
15. Kang, S. W. & Mueller, J. Multiscale 3D printing via active nozzle size and shape control. *Sci. Adv.* **10**, 7772 (2024).
16. Roach, D. J. et al. Long liquid crystal elastomer fibers with large reversible actuation strains for smart textiles and artificial muscles. *ACS Appl. Mater. Interfaces* **11**, 19514–19521 (2019).
17. Kuang, X. et al. Advances in 4D printing: materials and applications. *Adv. Funct. Mater.* **29**, 2 (2019).
18. Kim, Y., Yuk, H., Zhao, R., Chester, S. A. & Zhao, X. Printing ferromagnetic domains for untethered fast-transforming soft materials. *Nature* **558**, 274–279 (2018).
19. Pojman, J. A. Frontal polymerization. in *Polymer Science: A Comprehensive Reference* Vol. 1–10, 957–980 (Elsevier, 2012).
20. Mariani, A., Fiori, S., Chekanov, Y. & Pojman, J. A. Frontal ring-opening metathesis polymerization of dicyclopentadiene. *Macromolecules* **34**, 6539–6541 (2001).
21. Robertson, I. D. et al. Rapid energy-efficient manufacturing of polymers and composites via frontal polymerization. *Nature* **557**, 223–227 (2018).
22. Aw, J. E. et al. Self-regulative direct ink writing of frontally polymerizing thermoset polymers. *Adv. Mater. Technol.* **7**, 9 (2022).
23. Ziaee, M., Johnson, J. W. & Yourdkhani, M. 3D Printing of short-carbon-fiber-reinforced thermoset polymer composites via frontal polymerization. *ACS Appl. Mater. Interfaces* **14**, 16694–16702 (2022).
24. Ziaee, M., Naseri, I., Johnson, J. W., Franklin, K. A. & Yourdkhani, M. Frontal polymerization and three-dimensional printing of thermoset polymers with tunable thermomechanical properties. *ACS Appl. Polym. Mater.* **5**, 1715–1724 (2023).
25. Kazemian, A., Yuan, X., Davtalab, O. & Khoshnevis, B. Computer vision for real-time extrusion quality monitoring and control in robotic construction. *Autom. Constr.* **101**, 92–98 (2019).
26. Wang, W. et al. A real-time defect detection strategy for additive manufacturing processes based on deep learning and machine vision technologies. *Micromachines***15**, 28 (2023).
27. Johnson, M. V. et al. A generalizable artificial intelligence tool for identification and correction of self-supporting structures in additive manufacturing processes. *Addit. Manuf.* **46**, 102191 (2021).
28. Roach, D. J., Rohskopf, A., Leguizamon, S., Appelhans, L. & Cook, A. W. Invertible neural networks for real-time control of extrusion additive manufacturing. *Addit. Manuf.* **74**, 103742 (2023).
29. Linde, E., Celina, M. C., Appelhans, L. N., Roach, D. J. & Cook, A. W. In situ characterization of material extrusion printing by near-infrared spectroscopy. *Addit. Manuf.* **63**, 103420 (2023).
30. McDougall, L. et al. Free-form liquid crystal elastomers via embedded 4D printing. *ACS Appl Mater. Interfaces* **15**, 58897–58904 (2023).
31. Roach, D. J. et al. Utilizing computer vision and artificial intelligence algorithms to predict and design the mechanical compression response of direct ink write 3D printed foam replacement structures. *Addit. Manuf.* **41**, 101950 (2021).
32. Migler, K. B., Son, Y., Qiao, F. & Flynn, K. Extensional deformation, cohesive failure, and boundary conditions during sharkskin melt fracture. *J. Rheol.***46**, 383–400 (2002).
33. Inn, Y. W., Fischer, R. J. & Shaw, M. T. Visual observation of development of sharkskin melt fracture in polybutadiene extrusion. *Rheol. Acta* **37**, 573–582 (1998).
34. Lessard, J. J. et al. Unraveling reactivity differences: room-temperature ring-opening metathesis polymerization (ROMP) versus frontal ROMP. *J. Am. Chem. Soc.* **146**, 7216–7221 (2024).
35. Davydovich, O. et al. Frontal polymerization of dihydrofuran comonomer facilitates thermoset deconstruction. *Chem. Mater.* **34**, 8790–8797 (2022).
36. Shieh, P. et al. Cleavable comonomers enable degradable, recyclable thermoset plastics. *Nature* **583**, 542–547 (2020).
37. Lundberg, D. J., Ko, K., Kilgallon, L. J. & Johnson, J. A. Defining reactivity-deconstructability relationships for copolymerizations involving cleavable comonomer additives. *ACS Macro Lett.* **13**, 521–527 (2024).
38. Lloyd, E. M. et al. Efficient manufacture, deconstruction, and upcycling of high-performance thermosets and composites. *ACS Appl. Eng. Mater.* **1**, 477–485 (2023).
39. Kobelev, V. Principles of spring design. in *Fundamentals of Springs Mechanics* 3–36 (Springer Nature Switzerland, 2024).
40. Tomooka, K., Miyasaka, S., Motomura, S. & Igawa, K. Planar chiral dialkoxysilane: introduction of inherent chirality and high reactivity in conventional achiral alkene. *Chem. Eur. J.* **20**, 7598–7602 (2014).
41. Shieh, P., Nguyen, H. V.-T. & Johnson, J. A. Tailored silyl ether monomers enable backbone-degradable polynorbornene-based linear, bottlebrush and star copolymers through ROMP. *Nat. Chem.* **11**, 1124–1132 (2019).
42. Zakoworotny, M. et al. Rheological modeling of frontal-polymerization-based direct ink writing of thermoset polymers. *Comput. Methods Appl. Mech. Eng.* **418**, 116565 (2024).
43. Hossain, M. T. & Ewoldt, R. H. Protorheology. *J. Rheol.***68**, 113–144 (2024).


## Acknowledgements

This work was primarily funded by the Department of Energy (Office of Basic Energy Sciences) as part of the Energy Frontier Research Center titled Regenerative Energy-Efficient Manufacturing of Thermoset Polymeric Materials (REMAT) under award number DE-SC0023457. Sandia National Laboratories is a multimission laboratory managed and operated by National Technology & Engineering Solutions of Sandia, LLC, a wholly owned subsidiary of Honeywell International Inc., for the U.S. Department of Energy's National Nuclear Security Administration under contract DE-NA0003525. This paper describes objective technical results and analysis. Any subjective views or opinions that might be expressed in the paper do not necessarily represent the views of the U.S. Department of Energy or the United States Government.

## Author contributions

E.B.M., A.J.G., and J.A.J. supported the initial idea development, study design, and theoretical framework (conceptualization). L.N.A., S.C.L., A.W.C., and D.J.R. led the conceptualization and provided oversight, mentoring, and leadership for the research team (supervision). N.S. secured financial support for the project (funding acquisition), with additional support from J.A.J., L.N.A., S.C.L., A.W.C., and D.J.R. E.B.M., L.M., L.N.A., S.C.L., A.W.C., and D.J.R. developed and applied the methods and protocols used (methodology). L.M. and D.J.R. developed and implemented computational tools (software), with support from A.W.C. E.B.M. and L.M. performed experiments and collected data (investigation), with support from D.R.D., A.J.G., A.C., and D.J.R. L.M., N.G., D.R.D., and D.J.R. managed the research data (data curation), with E.B.M. leading this effort. E.B.M. and N.S. ensured the accuracy and reproducibility of results (validation), with additional support from L.M., N.G., L.N.A., S.C.L., A.W.C., and D.J.R. E.B.M. created graphical representations and figures (visualization) and drafted the initial manuscript (original draft). All authors revised, refined, and responded to feedback on the manuscript (review and editing).

## Competing interests
The authors declare no competing interests.

## Additional information
**Supplementary information** The online version contains supplementary material available at https://doi.org/10.1038/s44334-025-00032-1.

**Correspondence** and requests for materials should be addressed to Devin J. Roach.